ACS OMEGA

Article

Cite This: ACS Omega 2019, 4, 3458−3468

http://pubs.acs.org/journal/acsodf

Preparation and Comparison of Reduced Graphene Oxide and Carbon Nanotubes as Fillers in Conductive Natural Rubber for Flexible Electronics

Antonio Capezza,[†] Richard L. Andersson,[*,†] Valter Ström,[‡] Qiong Wu,[†] Benedetta Sacchi,[§] Stefano Farris,[∥] Mikael S. Hedenqvist,[†] and Richard T. Olsson[*,†]

[†]School of Engineering Sciences in Chemistry, Biotechnology and Health, Fibre and Polymer Technology and [‡]School of Industrial Engineering and Management, Material Science and Engineering, KTH Royal Institute of Technology, SE-100 44 Stockholm, Sweden

[§]Department of Chemistry, University of Milan, Via Golgi 19, 20133 Milan, Italy

[∥]DeFENS, Department of Food, Environmental and Nutritional Sciences—Packaging Division, University of Milan, Via Celoria 2, 20133 Milan, Italy

Supporting Information

ABSTRACT: Conductive natural rubber (NR) nanocomposites were prepared by solvent-casting suspensions of reduced graphene oxide (rGO) or carbon nanotubes (CNTs), followed by vulcanization of the rubber composites. Both rGO and CNT were compatible as fillers in the NR as well as having sufficient intrinsic electrical conductivity for functional applications. Physical (thermal) and chemical reduction of GO were investigated, and the results of the reductions were monitored by X-ray photoelectron spectroscopy for establishing a reduction protocol that was useful for the rGO nanocomposite preparation. Field-emission scanning electron microscopy showed that both nanofillers were adequately dispersed in the main NR phase. The CNT composite displays a marked mechanical hysteresis and higher elongation at break, in comparison to the rGO composites for an equal fraction of the carbon phase. Moreover, the composite conductivity was always ca. 3−4 orders of magnitude higher for the CNT composite than for the rGO composites, the former reaching a maximum conductivity of ca. 10.5 S/m, which was explained by the more favorable geometry of the CNT versus the rGO sheets. For low current density applications though, both composites achieved the necessary percolation and showed the electrical conductivity needed for being applied as flexible conductors for a light-emitting diode.

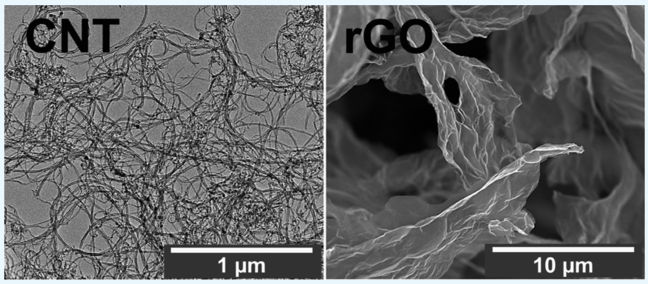

INTRODUCTION

Graphene and reduced graphene oxide (rGO) sheets consist of hexagonally arranged layered aromatic lattices, typically sized 2−5 μm laterally with a thickness of 2−3 nm, which are held together by sp^3 σ−C−C and sp^2-hybridized carbon atoms forming a π bond.[1] The bonds allow electron conduction within the sheets at an estimated speed of 1000 $cm^2\ V^{-1}\ s^{-1}$, making this allotrope of carbon interesting as a filler in polymers for preparation of conductive lightweight polymer nanocomposites.[2−4] However, although its sheet morphology with in-plane conduction may show excellent intrinsic conductivity, any composite conductivity on a larger scale is essentially based on a reliable network formation of the sheets. The rGO will here inevitably show fewer contact points as compared to randomly organized high-aspect-ratio rod-like fillers, for example, carbon nanotubes (CNTs).[5] It is thus of general interest to investigate the possibilities and limitations of graphene as a filler material to generate conductive polymer composites for soft material applications, such as materials for electrical insulation,[6] minimal static charge build-up,[7,8] and to even electrical conduction with charge transfer, for example, within electronics.[9−11]

The interest in rGO as a nanofiller material is further motivated considering the often limited conductivity of graphene and rGO in composites due to the nematic phase formation caused by partial phase separations of the rGO sheets in solution.[12] It is here of relevance to compare rGO with CNT as conductive fillers because CNTs have been demonstrated to form percolating networks at a volume fraction as low as 0.00125 vol %, that is because of the long slender morphologies of the CNTs.[13] A simple comparison with CNTs is however not straight forward because of the wide range of resistivity values reported for the graphene sheets obtained as rGO. This is because the conductance in any

Received: December 26, 2018
Accepted: February 5, 2019
Published: February 15, 2019

DOI: 10.1021/acsomega.8b03630
ACS Omega 2019, 4, 3458−3468

percolating carbon filler network also depends on the intrinsic conductivity of the individual sheets, which strongly depends on the reduction route.[14] Reductions of GO to rGO rely on the chemically or thermally assisted removal of hydroxyl, epoxy, carbonyl, and carboxyl groups, which often yields only partially rGO.[15,16] Comparative measurements on identically processed well-defined carbon-based fillers, such as CNTs, in relation to rGO obtained from a proven effective reduction protocol (ensuring reproducible high intrinsic conductivity within the sheets) will here provide valuable insights into the graphene performance as a carbon filler.[14]

In this article, we describe the preparation of rGO/natural rubber (NR) and CNT/NR nanocomposites by solvent casting followed by cross-linking of the formed conductive NR nanocomposite. NR was chosen as a high-performance elastomer because of its unique elastic properties, which allow for a complete recovery after significant deformation, for example, 400% stretching. For this reason, NR is a promising material even for applications that are beyond the tire industry,[18] such as flexible electronics.[17,18] The possibility to integrate the two nanofillers (CNTs and rGO) by simple solvent-based mixing, without using physical mixing techniques such as internal mixing, was investigated. The electrical performance of the resulting NR composites was then compared and evaluated. The electrical performance of identically processed CNTs/NR and rGO/NR composites revealed 1000 times higher conductivity for the same filler content when using commercial CNTs. However, the preparation method allowed for reaching sufficient electrical percolation to run a light-emitting diode (LED) for both the rGO and CNT composites (ca. minimum conduction: 10^{-4} S/m). Mechanical tests coupled with electrical tests were also performed to gather information about the strain history of the material as displayed by electrical measurements. A previously unreported electrical and mechanical hysteresis effect was observed for the CNT nanocomposites, opening for the obtained composites to be used as flexible strain memory sensors.

EXPERIMENTAL SECTION

Chemicals. GO prepared via the Hummer method[19] was supplied by Angstrom Materials, USA, as a suspension (solid content 0.5 wt %), reference number N002-PS, containing 46 wt % carbon, 46 wt % oxygen, 3 wt % hydrogen, and 0.5 wt % nitrogen. According to specification, more than 90% of the sheets had a lateral size above 1.2 μm. Multiwall CNTs (grade Flotube 700, purity ≥ 93%, average diameter of 6−8 nm, and a length up to 50 μm) were delivered by CNano Technology Limited, Beijing, China. The reducing agent sodium borohydride ($NaBH_4$) was obtained as ≥98% powder from Aldrich Chemistry and sodium hydroxide (NaOH, ≥97%) was supplied by Alfa Aesar. Ammonium hydroxide was 28−30% by concentration, reagent grade from Sigma-Aldrich. The NR was tapped from *Hevea brasiliensis* trees, coagulated by formic acid, precompounded in Malaysia, and supplied as 10CV60 by Syarikat Chuan Lee Rubber SDN. BHD., Malaysia. Zinc oxide (99.8% purity) and reagent grade sulphur (≥99.5%) were obtained from VWR. Stearic acid (≥97%) was purchased from Merck, and *N*-cyclohexyl-2-benzotiazolsulfenamide (CBS, >99.5%) was delivered by Henan Hengrui Rubber Plastic Science. Tetrahydrofuran (THF, ≥99.7%) was purchased from VWR International, toluene (≥99.5%) and acetone (≥99.9%) were obtained from Fisher Chemical, *n*-hexane (purity ≥97%) and *p*-xylene (purity ≥99%) were purchased from Sigma-Aldrich, and dichloromethane or chloroform was supplied from Merck Eurolab (≥99%). Ultrapure reagent type-1 water was used unless otherwise noted.

Preparation of Thermally rGO. Two methods of thermal reduction of GO were used: (i) a low-temperature treatment inside a vacuum oven at 150 °C for 60 min, (ii) a high-temperature process at 1000 °C for 5 s. For both of these processes, the 0.5 wt % GO suspension was first freeze-dried into a porous foam, which was subsequently placed inside a polypropylene Eppendorf test tube or a quartz tube for the low- and high-temperature treatment, respectively. The final foam of rGO was analyzed with X-ray photoelectron spectroscopy (XPS) to determine its elemental composition.

Preparation of Chemically rGO. The chemical reduction of GO was performed for comparison to the thermal route (above). To this scope, 2 mL of the 0.5 wt % GO suspension was placed into 10 mL glass vials under magnetic stirring (900 rpm) at 50 °C (under air). The sodium borohydride ($NaBH_4$) reducing agent[20] was prepared separately as 3, 6, and 12 g/L aqueous solutions. For each 2 mL GO sample, a premixture of 3 mL of the prepared reducing agent solution and 100 μL buffer of 54 mM of sodium hydroxide or ammonia was added. The final concentrations of the components in the reaction vessels were 0.2 wt % GO with 44, 88, or 176 mM $NaBH_4$ and 54 mM NaOH or ammonia. The reduction process was carried out for 2 h under constant stirring. The rGO samples were washed from excess sodium and boron ions by three exchanges of the sample supernatant, using centrifugation at 12 100 relative centrifugal force (RCF) for 30 min, followed by redispersion in water. An aliquot of each sample was freeze-dried to evaluate the chemical composition by XPS. The effect of using different concentrations of $NaBH_4$ was evaluated by measuring the differences in electrical conductivity of compacted foams. The refined rGO−water dispersions were further solvent exchanged into the final solvents, using acetone as a solvent bridge (using the above centrifugation procedure). The final rGO concentration in the specific solvents used for preparation of the cast rubber solutions was adjusted to 0.5 wt %. The estimated surface area of the rGO sheets is 13 035 mm^2g^{-1}.[21]

Preparation of CNT Suspensions. The dry multiwalled CNTs were dispersed by ultrasonication into THF or toluene by using a Sonics Vibra-Cell VCX 750 ultrasonication probe (6 mm tip), for 10 min at 21% of the maximum power 750 W. The final CNT concentration in the solvents was adjusted to 0.5 wt %. A transmission electron microscopy (TEM) micrograph of the used CNT is shown in the Figure S1 (Supporting Information). The used multiwalled CNTs had lengths of ca. 40 μm, 20 nm thickness and a wall thickness of 8 nm. The estimated surface area of the CNT is 1 610 mm^2g^{-1}.[21]

Preparation of NR Solutions. A screening of different solvents for liquid mixing of the solvent-borne rGO sheets and CNT, and the NR matrix, was carried out for THF, toluene, *n*-hexane, *p*-xylene, dichloromethane, and chloroform as 5 vol % NR solutions. Two up-scaled separate master batches of dissolved rubber were prepared by addition of 50 mL of NR to 950 mL of the respective THF and toluene solvent (5 vol %). These master batches were passed through a Büchner no. 1 filter to remove particles remaining from the smoking and compounding of the NR in Malaysia. The resulting translucent solutions were corrected in concentration by addition of

DOI: 10.1021/acsomega.8b03630
ACS Omega 2019, 4, 3458−3468

solvent that evaporated during the vacuum-assisted filtration and were used for all subsequent experiments.

Preparation of Conductive Composites. The solvent-borne rGO or CNTs were mixed into the NR solutions together with the required additives used for vulcanization and homogenized for 5 min at 5000 rpm with an Ultra-Turrax homogenizer (IKA, D125 Basic), followed by ultrasonication of the solution in a traditional ultrasonication bath for 5 min. The vulcanization additives consisted of 5 phr (parts per hundred of the reagent per 100 g of NR) ZnO, 3 phr sulphur, 1 phr stearic acid, and 0.8 phr CBS in each solution (equivalent to 4.6 wt % ZnO, 2.7 wt % sulphur, 0.9 wt % stearic acid and 0.7 wt % CBS, respectively), relative to the amount of NR used. The final composition with regard to the carbonaceous phase was adjusted by adding different amounts of the master batches containing 0.5 wt % rGO or CNTs (above). The solutions were poured into square-shaped glass molds (20 × 20 cm^2) and left to dry at ambient conditions for 12 h. Infrared (IR) spectroscopy (PerkinElmer Spectrum 2000, equipped with a single reflectance attenuated total reflectance (ATR) MkII Golden Gate stage from Specac, Ltd., London, UK) was used to monitor and confirm complete evaporation of all solvents before the vulcanization. A uniform evaporation of the solvents resulted in ca. 300 μm thick rubber composite films. The films were rolled off the mold and placed in a standardized metallic mold for tensile test specimens (ISO 37:2005 Type 3, 50 mm overall length, 20 mm length of narrow region and 1 mm thickness) and were vulcanized under 30 kN of pressure at 145 °C for 1 h in a hot press (Fontijne TP400 with press plates 320 × 320 mm). The method is shown in Figure 1.

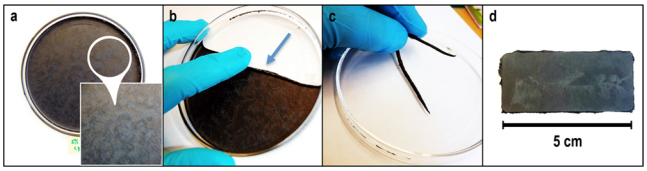

Figure 1. Preparation of the NR films by solvent casting. The films were left to dry after casting under normal atmosphere (a). Thereafter, they were rolled (b) into cylinders (c) and finally vulcanized into 50 × 10 mm sheets from the rolled probes (d).

Accordingly, all the conductive composites (rGO/NR and CNT/NR) were prepared by the above solvent mixing technique, using the same vulcanization time as established for a sample prepared by conventional mixing on a Banbury unit (see below).

To ensure that the solvent mixing process did not influence the physical properties of the rubber matrix (without any conductive nanofillers), a reference NR sample was compounded using a Banbury internal mixer, denoted as IM. The temperature during the mixing was controlled at 50−60 °C and the total compounding time was ca. 15 min. This sample was vulcanized under 30 kN of pressure at 145 °C for 1 h in a hot press (Fontijne TP400 with press plates 320 × 320 mm). The solvent mixed and the IM prepared samples are compared in Table 2, only containing the vulcanization agents.

Electron Microscopy. Cold field scanning electron microscopy was performed on a Hitachi S-4800. For the nonconductive samples, a Pt/Pd 60/40 alloy was sputtered onto the sample using a Cressington 208HR high-resolution sputter prior to the observation. TEM was performed on a Hitachi HT-7700 operated at 100 kV.

Electrical Characterization. The electrical conductivity of the CNT, GO, and rGO rubber films was evaluated on a Keithley 2400 SourceMeter connected to a collinear four-point probe setup (spacing 5 mm with gold plated 45° conical tips). The distance to any boundary was always more than 5 probe spacing's (>25 mm); thus, the analytical correction factor of $\pi/\ln(2)$ = 4.53 could be used without further modification in accordance to ASTM F 390. When measuring on the final vulcanized samples during the in situ mechanical/electrical testing, the conductivity was measured from four separate contact strips connected in a Kelvin bridge along the narrow section of the tensile testing specimens. The distance between the two inner sensing contacts was taken as the initial distance of the unstretched samples multiplied with the measured elongation recorded during the test. The cross-sectional area was calculated from a constant volume criteria during the tensile tests (Poisson's ratio ≈ 0.5),[22] and no grip slippage was observed.

XPS Analysis. XPS measurements were performed in an M-Probe instrument (Surface Science Instruments, USA) equipped with a monochromatic Al Kα source (1486.6 eV) with a spot size of 200 μm × 750 μm and a pass energy of 25 eV, providing a resolution for 0.74 eV. The energy scale was calibrated with reference to the $4f_{7/2}$ level of a freshly evaporated gold sample, at 84.0 ± 0.1 eV, and with reference to the $2p_{3/2}$ and 3s levels of copper at 932.47 ± 0.1 and 122.39 ± 0.15 eV, respectively. With a monochromatic source, an electron flood gun was used to compensate for the build-up of positive charge on the insulator samples during the analyses: a value of 10 eV was selected for these samples to be measured. For all the samples, the C 1s peak level was taken as the internal reference at 284.6 eV. The accuracy of the reported binding energies (BEs) can be estimated to be ±0.2 eV. Wide scan XPS survey spectra were used to gather information on the surface atomic composition of pristine GO samples and rGO samples. High-resolution spectra of C 1s was used to determine the carbon functionalities of GO and rGO.

IR Spectroscopy. IR spectroscopy was performed using a Spectrum 2000 Fourier-transform IR (FT-IR) spectrometer (PerkinElmer Inc., USA). A total of 16 scans were recorded. The Spectrum 2000 was equipped with a Golden Gate (Specac Ltd.) single reflection ATR accessory mounting a diamond crystal. All samples were placed in a desiccator for at least 1 week before the analyses.

Tensile Testing. Tensile testing of the rubber samples were carried out in an Instron 5566 mechanical tester in conjunction with a Keithley 2400 SourceMeter to acquire the in situ conductivity during the tensile tests. The strain rate was 20 mm/min, and all samples were conditioned at 23 °C and 50% RH for 14 days prior to each test. The specimens had a shape and size according to ISO 37:2005 Type 3, see previous paragraph.

RESULTS AND DISCUSSION

Morphology after Reduction to rGO. The starting material GO used for the evaluation of different reduction routes, as well as the rGO, is shown as freeze-dried porous powders in Figure 2. The GO sheets seen inside the freeze-dried foam had a size of ca. 5 μm on average, with the largest sheets sized up to ca. 10 μm, see Figure 2a. Because of the even sublimation of the aqueous phase during the drying, no apparent density gradient could be observed in the foam structure, and the volume of the 1 mL suspension of GO was

DOI: 10.1021/acsomega.8b03630
ACS Omega 2019, 4, 3458−3468

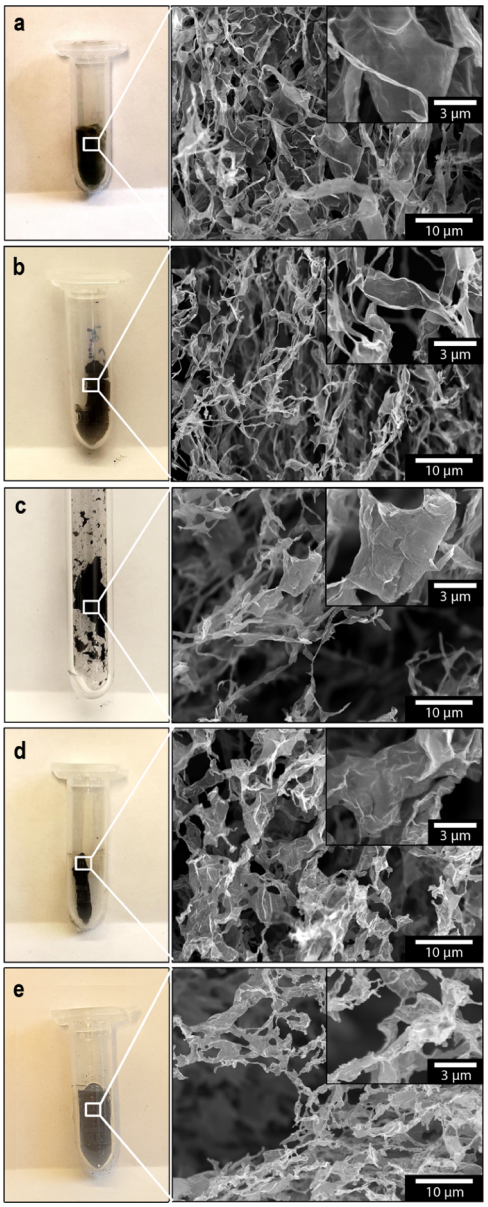

Figure 2. Micrograph showing GO and rGO sheets after 72 h of freeze-drying. (a) GO, (b) reduced GO at 150 °C in vacuum (60 min), (c) high-temperature reduction at 1000 °C (5 s), (d) chemically reduced GO (NaOH buffer), and (e) chemically reduced GO (NH_4OH buffer).

largely preserved after the freeze-drying was completed. The preservation and stabilization of the shape, as remnants from the frozen GO solution, was previously documented as a result of the high content of oxygen present on the sheets, which also facilitates a high degree of dispersion the GO in the aqueous state before the freezing operation.[23] The rGO produced by the low-temperature vacuum oven reduction at 150 °C for 60 min (Figure 2b) was to some extent also able to maintain its foam structure during the freeze-drying operation, although the individual graphene sheets were crumbled at their edges and the overall internal morphology was comprised of more narrow sheets (ca. 100 nm wide), with the widest sheets reaching ca. 1.5 μm in width (Figure 2b, inset). Larger sheets associated with the GO sample were completely absent. Similarly, the rGO from the high-temperature reduction at 1000 °C for 5 s (Figure 2c) also crumpled in the same fashion, whereas larger sheets could be observed in the sample (Figure 2c inset). However, a complete collapse of the foam occurred during the rapid 5 s heat exposure, as seen in the photograph, resulting in a heavily aggregated material. It should be noted that all the thermally heat-treated samples had the shape and porosity of the GO sample in Figure 2a before the thermal treatment.

Figure 2d shows the result of freeze-drying the chemically reduced GO, after using NaOH as buffering solution at a $NaBH_4$ concentration of 176 mM. The sheets of the rGO were also for the chemically reduced system severely contracted and crumbled along their edges, indicating a successful reduction (similar to the thermally treated samples). The entire foam was however severely contracted after drying (photograph, Figure 2d) and the foam decreased to ca. 50% of its initial volume before the freeze-drying, that is, forming a more dense foam in agreement with previous results by Guex et al.[23] In comparison, the GO reduced using NH_4OH as a buffer displayed the most uniform rGO foam morphology (Figure 2e) among all the reduced samples, with almost a complete absence of sample shrinkage during the freeze-drying. The small contraction of the sample was explained by the stabilizing effect that NH_4OH had on the sheets in their suspended state. In fact, the ammonia contributed to a dispersed rGO phase that was not possible to separate from the solution by centrifugation at 12 100 RCF for 30 min, that is, as tested before the freeze-drying evaluation. The individual sheets were however similar in morphology with the sheets obtained using sodium hydroxide as buffer solution.

XPS of rGO. Wide scan XPS spectra of the GO and the rGOs allowed the determination of the oxygen/carbon elemental percentage proportions (Table 1). The elemental composition of GO included carbon and oxygen at an atomic percentage of 69.64 and 30.36 atom %, respectively, in line with recent literature data (C/O value of 2.29).[23−25] High-resolution C 1s spectrum of GO (Figure 3a) exhibited a saddle-like pattern, which is a signature of a significant oxidation of the GO sheets, which stemmed from their exfoliation process from the graphite.[26] Deconvolution of the C 1s peak in GO disclosed the presence of the following

Table 1. Elemental Surface Analysis and C/O Atomic Ratio of Graphene Oxide (GO1), Thermally Reduced at 150 °C × 1 h under Vacuum (GO2), Thermally Reduced GO at 1000 °C × 5 s (GO3), Chemically Reduced GO Using $NaBH_4$ + Ammonia (GO4), and Chemically Reduced GO Using $NaBH_4$ + NaOH (GO5) Samples Determined by XPS

sample	treatment	C	O	Na	B	C/O
GO1	pristine	69.64	30.36			2.29
GO2	vacuum reduced (150 °C, 12 h)	81.97	18.03			4.55
GO3	thermally reduced (1000 °C, 5 s)	83.57	16.43			5.09
GO4	chemically reduced ($NaBH_4$ + NH_4OH)	75.11	19.30	2.83	2.76	3.89
GO5	chemically reduced ($NaBH_4$ + NaOH)	85.24	12.67	2.09		6.87

DOI: 10.1021/acsomega.8b03630
ACS Omega 2019, 4, 3458−3468

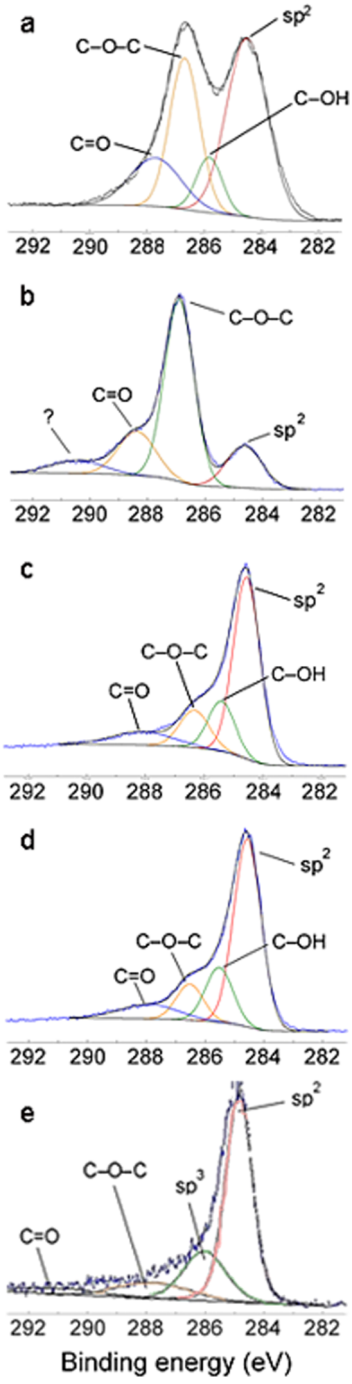

Figure 3. High-resolution deconvoluted C 1s XPS spectra of (a) GO, (b) thermally reduced at 150 °C, (c) thermally reduced GO at 1000 °C, (d) chemically reduced GO using $NaBH_4$ + ammonia, and (e) chemically reduced GO using $NaBH_4$ + NaOH.

functional groups: hydroxyl, carbonyl, and epoxy groups, the latter being the most representative (Table S1, Supporting Information).[14] At first glance, the high-resolution C 1s spectrum of all the reduced GO samples exhibited a shift from the double peak seen for the pristine GO to a single sharp peak, which indicates the formation of the sp^2 bonding graphene structure.[26] The high-resolution C 1s spectrum obtained from the vacuum-reduced GO sample (150° for 1 h) is displayed in Figure 3b and shows that the band at 284.6 eV decreased in intensity, with a proportional increase of the band centered at 286.9 eV, which was assigned to the epoxy (C−O−C) functionalities.[26−33] In particular, ensuing from the fitting procedure of the C 1s XPS spectra, the C−O−C functionalities in the vacuum-reduced GO sample accounted for the 58.45% of the total, while the nonfunctionalized carbon represented the 16.45% (Table S1). This was reflected in a C/O value of 4.55 and an oxygen content of 18.03%. Moreover, a small peak at 290.4 eV was also present in the spectra. This has previously been ascribed to as a ($\pi \rightarrow \pi^*$) shakeup satellite peak at ∼290.5 eV, indicating that delocalized π conjugation, a characteristic of aromatic C structure, is to some extent restored in heat-treated GO samples.[29,30,34] In comparison, the thermal reduction of GO at 1000 °C for 5 s (Figure 3c) provided an extensive GO reduction in consideration to carbon and oxygen atomic percentage, which were 83.57 and 16.43 atom %, respectively, yielding a C/O ratio of 5.09 (Table 1).

The reduction using $NaBH_4$ with ammonia resulted in a C/O value of 3.89, that is, a decrease in the oxygen content to 19.30 at. % (Table 1), in agreement with what was reported by Dave et al.[24] and a ca. 20% higher concentration of oxygen compared to the results from the high-temperature reduction. In addition, a higher percentage of nonfunctionalized carbon, that is, C−C and C═C (Table S1) was observed (61.1% compared to 48.7% of GO).

Interestingly, the use of $NaBH_4$ in combination with ammonia was very effective in depressing the carboxyl functionalities, which could not be detected in the sample (Figure 3d, Table S1). The wide scan XPS spectra of GO reduced with NaOH and $NaBH_4$ showed also a decrease in the surface oxygen content compared with the pristine GO (Table 1), yielding the highest C/O value among the sample tested in this work (C/O ratio 6.87). This was supported by the overall view of the C 1s XPS spectra in Figure 3e, where the main peak at ca 286.7 eV completely disappeared (only a subtle bump was observed at the same BE) because of the reduction of both epoxy and carbonyl functionalities (see Table S1).

Overall, the different reduction routes revealed the thermal treatments as very efficient, providing high C/O ratios: 4.55 and 5.09 for 60 min under 150 °C (vacuum) and for 5 s at 1000 °C (air), respectively. However, with the unavoidable aggregation of the sheets during the elimination of the aqueous phase, only the chemically reduced GO showing C/O ratios of 3.89 and 6.87 (ammonia and NaOH, respectively) was selected for further evaluation, thus eliminating the need for additional drying steps prior to mixing with the NR solutions. Here, an evaluation of smaller concentration of $NaBH_4$ reducing agent was performed, for both the ammonia and the NaOH buffer, to study the evolution of the C/O ratios during the chemical reduction of GO into rGO, and to ensure that the reduction had reached its maximum conversion for the employed reaction conditions, see Figure 4.

Figure 4 shows the increase in conductivity of the chemically reduced rGO as related to the amount of $NaBH_4$ concentration in the reducing buffer solution of sodium hydroxide or ammonia. All the reductions were carried out at 50 °C for 2 h, followed by 12 h at room temperature to ensure as complete reduction as possible for the given amount of reducing agent ($NaBH_4$). The concentrations of the buffer solutions were here equally set to 54 mM to prevent premature decomposition of the reductant.[17] From the results, it can be seen that the concentration of the reducing agent had a significant impact on the overall conductive properties of the obtained rGO,

DOI: 10.1021/acsomega.8b03630
ACS Omega 2019, 4, 3458−3468

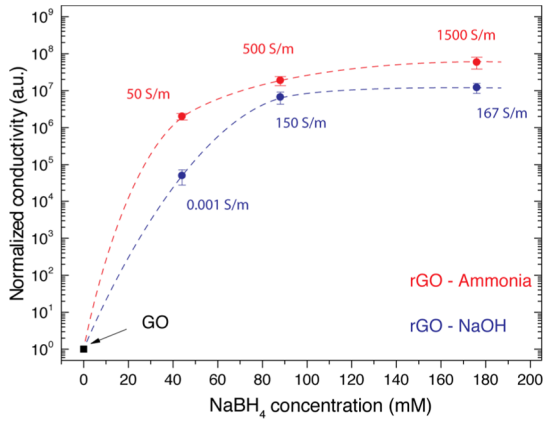

Figure 4. Change in conductivity of dried films of the rGO with an increasing amount of the reduction agent, $NaBH_4$. Dashed red/top line refer to system reduced by ammonia as buffer, blue/bottom line refers to when using sodium hydroxide as buffer. All reductions were carried out as 2 h reactions at 50 °C, followed by 12 h at room temperature.

showing a ca. 8 orders of magnitude increase in conductivity compared with the nonreduced GO sample and a variation in ca. 4 orders of magnitude depending on the reducing agent concentration. The explanation to the lower conductivity of 180 S/m for the NaOH-buffered system (as compared to earlier reported 1500 S/m value also obtained with a 54 mM NaOH buffer)[23] was a less extensive reduction because of the reaction temperature set to 50 °C instead of 80 °C, in combination with the sodium borohydride concentration equivalent to only ca. 60 wt % of what was previously reported (300 mM).[23] Interestingly, the presence of ammonia as a buffer solution generated consistently lower values of resistivity (higher conductivity) for identically formed films. In fact, the ca. 1500 S/m value reached for the 176 mM $NaBH_4$ solution at 50 °C was on a par with the reduction obtained using sodium hydroxide as buffer solution at 80 °C at a 300 mM concentration of $NaBH_4$, that is, almost twice as high concentration. The results demonstrate that ammonia assists in more efficient reduction for a given amount of $NaBH_4$ although with the drawback that the ammonium hydroxide stabilizes the rGO as a suspended phase (after the reaction) that could not be separated using a conventional centrifuge (see morphology section). For comparison, the thermally reduced samples showed resistivity values corresponding to conductivities of 50 and 12.5 S/m for the vacuum oven reduced at 150 °C and the 1000 °C (5 s) samples, respectively. However, the values could not be compared with the filtered samples from chemical reduction because a 4-probe measurement could not be conducted in a reliable manner over the compressed samples that were not behaving as continuous films.[23] In essence, a considerable portion of the conjugated bonded oxygen, epoxide, and amine groups present on the pristine GO had in both aqueous reductions been removed from the surface the GO, which resulted in a substantial increase in the "sheet-assembly" conductivities from ca. 8×10^{-6} S/m[23] to as much as 1500 S/m.[23] However, the ability of ammonia to stabilize the rGO in the aqueous suspensions to an extent that it was not possible to separate the rGO from the pitch-black solution resulted in that all the proceeding experiments were limited to the GO reduced in the presence of NaOH buffer solution. The GO reduced with the NaOH buffer was accordingly solvent exchanged into THF, chloroform, toluene, and hexane, via a first solvent exchange from water to acetone for the purpose of solution mixing the reduced GO with the dissolved NR solution (using the same solvents).

Evaluation of Protocol for Solution Blending the Solvent-Borne Carbon Fillers with Dissolved NR. Among the solvents tested only THF and toluene demonstrated satisfactory results with complete dissolution of the NR in the absence of severe flocculation of the vulcanization additives before and after the vulcanization. Figure 5 shows the IR

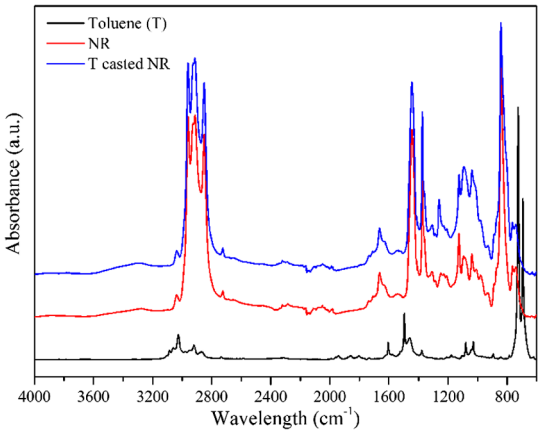

Figure 5. FT-IR spectra for the dry cast NR film dissolved in toluene, raw material rubber, and toluene (T) spectrum are shown.

spectroscopy analysis results of the cast dry film of NR obtained using toluene in absence of any filler phase (after 48 h) together with the raw rubber material cut from the larger piece delivered to from the manufacturer. The FT-IR was measured to ensure that the solvent mixing method had no influence on the preparation on the rubber matrix, that is, affecting the rubber structure.

It was confirmed that the dissolved and dried rubber showed identical spectra with the spectra for the raw rubber material from the manufacturer (reference sample) and no changes in the peak intensities could be observed. The FT-IR data also confirmed that the characteristic peaks of the solvents (at 600−800 cm^{-1}) were not present in the rubber spectra after drying. The result was repetitive for the THF sample. The nondestructive nature of the solvent mixing procedure was further confirmed by including all the vulcanization components (in absence of the carbon filler phase), followed by drying and vulcanization at 145 ° C for 1 h and comparing the mechanical data with a rubber prepared by traditional physical mixing (IM) on a Banbury unit (followed vulcanization), using tensile testing. The results revealed strain and stress values for 100, 200, and 300% strain and showed all values within 10% deviation between samples (see Table 2), and maximum strain values exceeded 550% for stress values of ca. 20 MPa, which is in agreement with previously reported literature values.[35,36] Only a small increase in the moduli of the toluene-based samples [as compared to the samples prepared by traditional mixing (IM)] could be observed (see, Table 2). This difference was suggested to stem from an improved dissolution of the sulphur phase because toluene is a better solvent of sulphur, as compared to THF.[25,26]

DOI: 10.1021/acsomega.8b03630
ACS Omega 2019, 4, 3458−3468

Table 2. Tensile Properties for the Cast and Vulcanized NR at 145 °C for 1 h[a]

sample		strain (%)	stress (MPa)
IM	moduli	100	1.23 ± 0.03
THF			1.22 ± 0.02
toluene			1.30 ± 0.03
IM		200	2.10 ± 0.05
THF			1.95 ± 0.08
toluene			2.43 ± 0.03
IM		300	3.10 ± 0.20
THF			2.88 ± 0.09
toluene			3.95 ± 0.07
IM	break	741 ± 30	25.0 ± 3.0
THF		709 ± 20	19.0 ± 3.0
toluene		578 ± 19	15.0 ± 3.0

[a]A reference sample compounded in an IM and vulcanized under the same conditions as the cast rubber is shown (IM). Moduli values are representing stress values in MPa required to strain the samples to different elongations, in accordance w. ISO standard 37.

Electrical Properties Post Vulcanization of the Solvent Cast Rubber with rGO or CNT. The rGO sheets are shown in Figure 6a, whereas the multiwall CNTs with an average diameter of 6−8 nm and length up to 50 μm are shown in Figure 6b with the same magnification. Figure 6c shows that depending on the solvent used to prepare the rGO nanocomposites (THF or toluene), the final composite conductivity varied by ca. 2 orders of magnitude for identically processed samples. Using toluene resulted in composites always showing higher conductivity compared with the THF (Figure 6).

The internal morphology of the nanocomposites was investigated from freeze-fractured surfaces of the 0.5 wt % rGO composites (Figure S2). The rGO−toluene composite displayed a completely homogeneous structure, whereas the rGO−THF-based material showed inclusions embedded in the rubber matrix (Figure S2, left). The structures were likely to be sulphur crystals remaining intact inside the vulcanized composite because of the lack of high-shear mastication. Also, because of a higher solubility of the sulphur particles in toluene, smaller inclusions were present in the rGO−toluene-based composites (Figure S2, right),[35,37] which suggested that most sulphur had dissolved prior to the solvent casting and vulcanization. However, the inhomogeneity observed in Figure S2 could also be a combination of the other vulcanization agents used in the rubber formulation. The composites containing CNTs as comparison were therefore only prepared from toluene (Figure 6). The difference in conductivity between rGO−toluene and the CNT−toluene composites was significant. The CNT-based composites showed the percolation threshold already at ca. 1 wt % CNT content, while only a small linear increase in conductivity could be observed up to 7−8 wt % for the rGO composites. Overall, the more beneficial shape of the high-aspect-ratio CNT rods resulted in a significantly improved conductivity compared with the most conductive rGO samples at any given concentration, which at its most displayed as 5 orders of magnitude difference for the composites containing 4.4 wt % rGO and CNTs, showing 9.4 × 10^{-5} and 0.47 S/m, respectively. The highest conductivity was in relatively good agreement with conductive data reported by Wang et al. for NR composites of CNTs where cellulose crystals were used

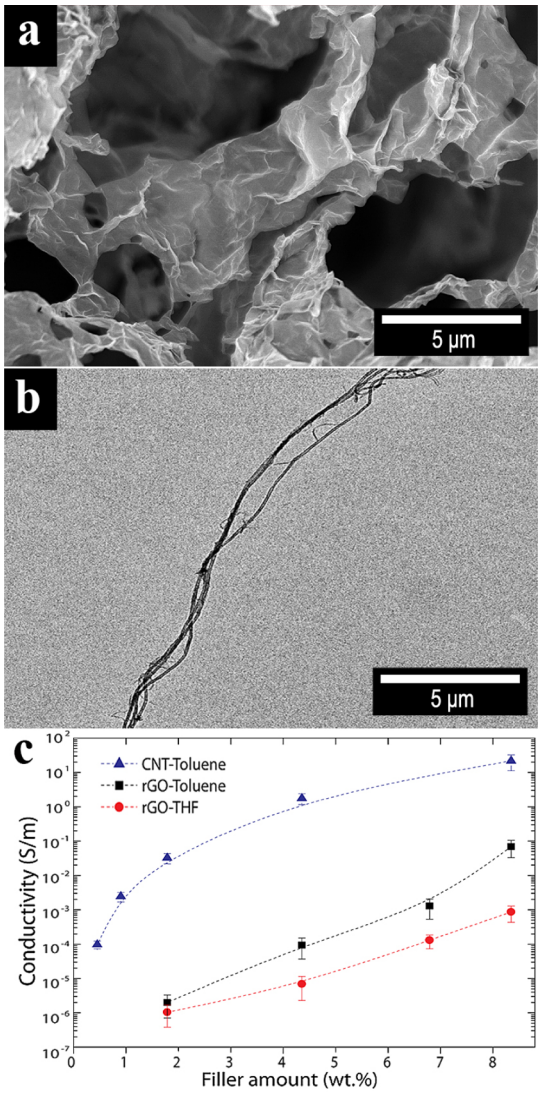

Figure 6. Reduced GO and the multiwall CNTs used for the rubber composites (a,b) and the normalized conductivity with increasing the wt % of rGO and CNT in the NR matrix for toluene and THF solvents (c).

effectively to assist in the formation of percolating networks, although the percolation threshold was herein observed at lower values.[38] A limited early percolation for graphene-containing polymer nanocomposites has previously been related to possible self-assembly of graphene sheets into nematic phases below the onset of percolation because of their flat anisotropic morphology.[12,21] In comparison to the data reported by Potts et al. and Kuilla et al.,[18,39,40] who demonstrated rGO percolation in polymers at 0.2−2 vol % (corresponding to 0.08 to 0.8 wt %), the established conductivity values at 2−4 wt % were however comparatively low because no apparent strong agglomerates were visible in the rGO composites' cast from toluene. A 0.1 vol % solution of NR was therefore added to dispersions of rGO in both toluene and THF to investigate the nature of the interaction between the rGO and the solvent prior to extraction of the solvents. The suspension generated a stable black mixture immediately on mixing the components, which was in contrast to the instability of the rGO in the pure solvents. The composite suspension remained stable and showed no phase separation or

DOI: 10.1021/acsomega.8b03630
ACS Omega 2019, 4, 3458−3468

sedimentation of the rGO phase for 3 months (Figure S3). The strong stabilizing effect of the rGO sheets (by absorption of the NR isoprene molecules on the surface of the rGO) may also have limited possibility of having rGO flake-to-flake contact points, and thus limited conduction. Nonetheless, this result proves that the addition of low amount of dissolved NR to rGO dispersed in organic solvents improved the stability of the nanofiller suspension and may thus be used as a possible surface modification agent of the nanosheets in nonpolar solvents. Figure 7a shows the surface morphology of the cryo-

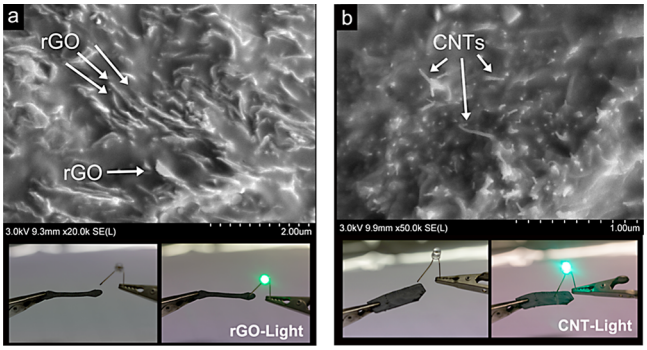

Figure 7. Field emission scanning electron microscopy images of the conductive rGO/NR (a) and CNT/NR (b) with 8 wt % filler content. An LED was used to illustrate the conductivity of the samples.

fractured samples with 8 wt % rGO. Not only a dominant parallel orientation of the embedded rGO sheets (Figure 7a) but also 100−200 nm separations of the sheets with insulating NR between could be observed. Figure 7b shows the morphology associated with the more randomly oriented CNTs with 8 wt % CNT concentration. In both cases, the conduction of the composites was sufficient to light a LED at 8 wt % filler content.

Dynamic Electrical Properties of the Solvent Cast Rubber with CNT. The NR nanocomposite with 8 wt % CNT filler was mechanically tested with simultaneous recording of its electrical resistivity to investigate how the electrical properties were affected by stretching the samples (Figure 8). The 8 wt % CNT sample was selected because the concentration was above the percolation threshold for the CNT nanocomposites and also because it represented the most conductive composite among the others. The dynamic electrical and mechanical properties of the 8 wt % rGO/NR composite is not shown because of its limited flexibility and early fracture, as a consequence of the challenging dispersion of the rGO nanofiller in the rubber matrix. Furthermore, the ca. 3 orders of magnitude lower conductivity presented by the rGO/NR samples was not sufficient to be measured accurately in the setup designed for this experiment.

The conductive rubber was repeatedly stretched with increasing deformation until failure (Figure 8a). The maximum strain of 580% at 20 MPa stress was rather high for a filled NR system, indicating a successful dispersion of the CNT phase. Previous works on filled NR reported a maximum strain of ca. 700 and 300%, for 1 and 7% filler contents, respectively.[35] The homogeneous dispersion of the CNTs within the NR matrix was also reflected in the high elastic recovery of the material deformation for strain values from 25 to 50%, which indicated that permanent phase segregation zones (volumes) were very small (Figure 8a). For comparison, the dynamic mechanical

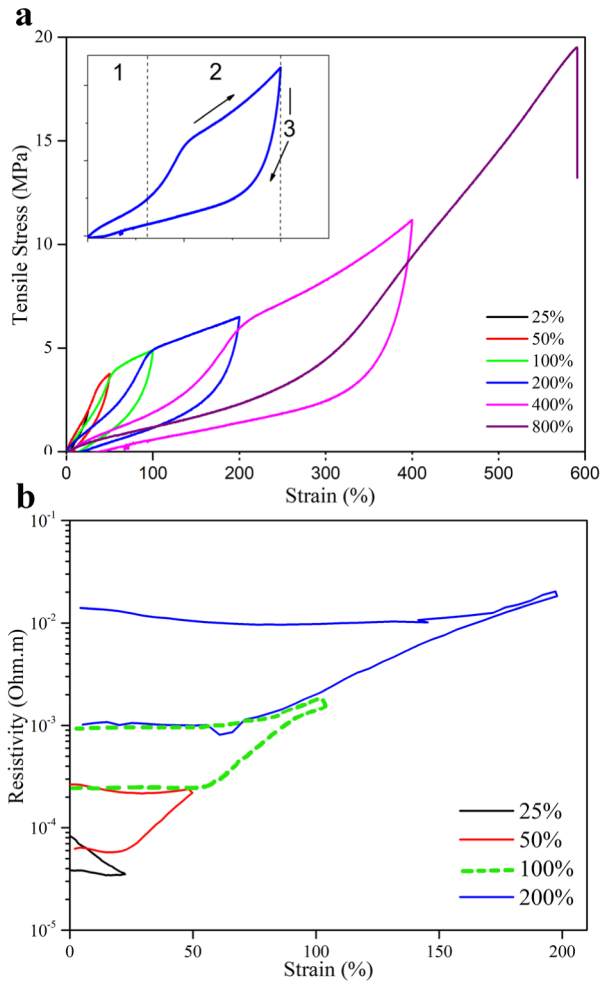

Figure 8. Strain−stress curves for CNT/NR (a) with 8 wt % filler content and the simultaneous resistivity cycles after each stretching event for the same CNT/NR sample (b).

stretching of the second most filled rGO/NR (i.e., 4.4 wt % rGO) is shown in Figure S4. The same cycles for higher rGO contents were not possible to measure and hence are not shown. The 4.4 wt % rGO/NR composites showed the inferior distribution of the carbon phase, resulting in a maximum strain value of 150% and an associated early failure of the composites. A possible strong interaction between the rGO and the NR molecules during the vulcanization process because of the known remaining oxygen functionalities on the surface of the rGO may have also influenced the flexibility of the sample.[23] Moreover, the rGO had seven times higher estimated surface area than the CNT filler, as shown in the experimental. Similar mechanical data describing maximum strain values in the 100−120% region was previously observed by Lin et al., utilizing a phase segregated graphene/NR composite morphology to effectively reduce the content of graphene.[41] However, the favorable interaction within the CNTs/NR system is displayed as extensive hysteresis loops for all the prepared CNT samples. The hysteresis characteristic of the CNT/NR system is typically referred to as the Müllins effect, reflecting an extensive formation of new surfaces inside the composites, that is, as the well-dispersed filler is perturbed in its interaction with the polymer matrix.[42,43] The Mullin effect was observed for the CNT as well as the rGO filled composites (Figures 8

DOI: 10.1021/acsomega.8b03630
ACS Omega 2019, 4, 3458−3468

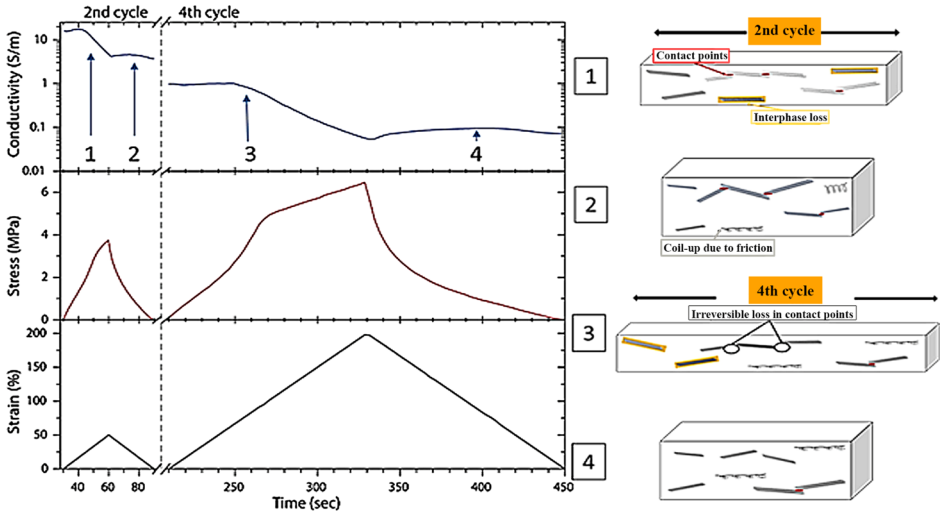

Figure 9. Conductivity properties of CNT/NR (toluene-based) when applying stretching cycles of 50 and 200%. (1,2) illustrate the suggested microstructural evolution for low strain and (3,4) for high strain after loss in contact points.

and S4). Figure S5 shows the absence of the effect for the neat NR, when stretched under identical conditions.

Figure 8b shows that although the electrical setup could only be used to accurately monitor the sample conductivity for repeated stretching up to 200%, the deformations were always associated with a partial conductivity loss (increase in resistivity) that remained for the composites, although their shape was completely recovered. The resistivity of the sample increased from ca. 5×10^{-5} to 1×10^{-4} ohm m with a 25% elongation from the original length, followed by an increase in resistivity from 3×10^{-4} to 8×10^{-3} ohm m with the second 50% elongation cycle. Finally, an increase from 1×10^{-3} to 9.5×10^{-1} ohm m was observed as the sample was stretched for the third time to 200% of its original length (Figure 8b). The hysteresis loops showed in Figure 8 are commonly related to the generation of voids in the samples because of the breakage of the network within the nanocomposite. However, the void formation could not be the entire mechanism in this case because the collapse of such voids during the relaxation stage would promote a partial decrease in the resistivity, as the conductive filler would come into contact again. Density measurements on the tensile tested samples were therefore made to check for any residual voids after tensile testing. No significant density changes were obtained from the samples before and after the tests. Furthermore, according to previous works, generation of voids should not affect the resistivity of the nanocomposite.[16,43] Consequently, it is suggested that partial slippage of the CNT nanofiller and subsequent bending/coiling processes occurred during relaxation stage. This would permanently reduce the number of contact points and therefore negatively affect the electrical conductivity of the sample. It is therefore suggested that the progressive increase in the hysteresis behavior was related to the conductive filler (consisting of a distribution of sizes, shapes, and orientations), wherein the first nanotubes that lost contact were smaller and completely aligned with the stretching direction, whereas the larger sized were entangled and lost contact at higher stretching values. The suggested mechanism is represented in Figure 9. Here, the conductivity remained constant in the linear stress−strain zone (1), whereas in the nonlinear zone from the tensile stress cure (2) the conductivity started to increase linearly (on the log axis) until the maximum elongation for the current cycle was reached. Finally, when the sample was unloaded, the conductivity remained constant and did not recover to the initial value in zone (1). Accordingly, a permanent damage in the percolation network of the CNTs had at this point occurred. This permanent damage increased when the sample was exposed to higher strain and further cycles as shown in Figure 9(3,4).

CONCLUSIONS

rGO was herein evaluated in comparison to multiwalled CNTs as a conductive filler for the preparation of a flexible, and simultaneously electrically conductive, NR material. To facilitate preparation of the most conductive NR formulation with highest possible conductivity of the rGO phase, solvent casting was used to favor the rGO filler dispersion after a comparison of four different routes to reach highest possible intrinsic condition of the rGO phase. The most useful reduction process of the GO sheets was identified as using NaOH as buffer in aqueous solution and $NaBH_4$ as reducing agent, followed by the solvent exchange process, to reach sufficient conductivity to light a LED diode. A strong association of the dissolved NR (polyisoprene) onto the rGO sheets dispersed in nonpolar solvents was suggested to partially explain a limited early percolation threshold for the rGO sheets as compared to CNTs, which only provided 1/1000 of the conduction compared with an equal amount of CNTs dispersed in an identical manner. The strong matrix adhesion was further supported by mechanical data, which showed that the flexibility of the NR matrix decreased from allowing a 600% maximum strain for a composite containing 8 wt % CNT to 150% for the composites containing solely 4.4 wt % rGO. In fact, the 8 wt % rGO/NR composites had lost all flexibility and fractured in the first strain cycle. The unfavorable shape factor of the rGO sheets as compared to the CNTs, as an elongated filler conductor, also must have played a role in the limited percolation of the rGO/NR composites. On the contrary, the favorable dispersion of the CNTs allowed preparation of a lightweight and flexible conductor from the most conductive CNT/NR composite system (displaying an initial 10.5 S/m conductivity), which revealed a permanent loss of its specific conductivity with each stretching cycle employed (up to 200% strain) via mechanical testing. The CNT/NR

DOI: 10.1021/acsomega.8b03630
ACS Omega 2019, 4, 3458−3468

material may therefore find use in applications such as inexpensive large-strain sensors, or integrated tyres pressure/vibration sensors, where the combination of flexibility and conductivity allow for recording repeated large-strain deformation in terms of its effect on the percolating CNT network.

■ ASSOCIATED CONTENT

Supporting Information

The Supporting Information is available free of charge on the ACS Publications website at DOI: 10.1021/acsomega.8b03630.

Additional information on the nature of the CNTs, XPS data, microscopy of fractured surfaces, stability of carbon fillers in dissolved NR, and tensile test cycles can be found in the Supporting Information (S1−S5 and Table S1) (PDF)

■ AUTHOR INFORMATION

Corresponding Authors

*E-mail: riander@kth.se (R.L.A.).
*E-mail: rols@kth.se. Phone: +46 8 7909426 (R.T.O.).

ORCID

Richard L. Andersson: 0000-0002-0236-5420
Stefano Farris: 0000-0002-6423-8443
Mikael S. Hedenqvist: 0000-0002-6071-6241
Richard T. Olsson: 0000-0001-5454-3316

Notes

The authors declare no competing financial interest.

■ ACKNOWLEDGMENTS

The authors acknowledge Prof. Natalia León and Prof. Rosestela Morales for the scientific feedback and valuable knowledge about rubber materials.

■ REFERENCES

(1) Warner, J. H.; Schaffel, F.; Rummeli, M.; Bachmatiuk, A. *Graphene: Fundamentals and Emergent Applications*; Newnes, 2012.

(2) Eigler, S.; Enzelberger-Heim, M.; Grimm, S.; Hofmann, P.; Kroener, W.; Geworski, A.; Dotzer, C.; Röckert, M.; Xiao, J.; Papp, C.; Lytken, O.; Steinrück, H.-P.; Müller, P.; Hirsch, A. Wet Chemical Synthesis of Graphene. *Adv. Mater.* **2013**, *25*, 3583−3587.

(3) Stankovich, S.; Dikin, D. A.; Dommett, G. H. B.; Kohlhaas, K. M.; Zimney, E. J.; Stach, E. A.; Piner, R. D.; Nguyen, S. T.; Ruoff, R. S. Graphene-based composite materials. *Nature* **2006**, *442*, 282−286.

(4) Matos, C. F.; Galembeck, F.; Zarbin, A. J. G. Multifunctional materials based on iron/iron oxide-filled carbon nanotubes/natural rubber composites. *Carbon* **2012**, *50*, 4685−4695.

(5) Zhan, Y. H.; Liu, G. Q.; Xia, H. S.; Yan, N. Natural rubber/carbon black/carbon nanotubes composites prepared through ultrasonic assisted latex mixing process. *Plast., Rubber Compos.* **2011**, *40*, 32−39.

(6) Pourrahimi, A. M.; Olsson, R. T.; Hedenqvist, M. S. The Role of Interfaces in Polyethylene/Metal-Oxide Nanocomposites for Ultrahigh-Voltage Insulating Materials. *Adv. Mater.* **2017**, *30*, 1703624.

(7) Nicolais, L.; Gigliotti, K. Static Electricity and Aircraft. In *Wiley Encyclopedia of Composites*; Nicolais, L., Ed.; John Wiley & Sons, Inc., 2012.

(8) Zhang, H.; Harwood, W.; Ross, G. Antistatic polymer monofilament, method for making an antistatic polymer monofilament for the production of spiral fabrics and spiral fabrics formed with such monofilaments. U.S. Patent 0,019,093 A1, 2006.

(9) Makled, M. H.; Sheha, E.; Shanap, T. S.; El-Mansy, M. K. Electrical conduction and dielectric relaxation in p-type PVA/CuI polymer composite. *J. Adv. Res.* **2013**, *4*, 531−538.

(10) Schneider, V.; Polonskyi, O.; Strunskus, T.; Elbahri, M.; Faupel, F. Light-induced Conductance Switching in Photomechanically Active Carbon Nanotube-Polymer Composites. *Sci. Rep.* **2017**, *7*, 9648.

(11) Juwhari, H. K.; Abuobaid, A.; Zihlif, A. M.; Elimat, Z. M. Investigation of Thermal and Electrical Properties for Conductive Polymer Composites. *J. Electron. Mater.* **2017**, *46*, 5705−5714.

(12) Yuan, J.; Luna, A.; Neri, W.; Zakri, C.; Schilling, T.; Colin, A.; Poulin, P. Graphene liquid crystal retarded percolation for new high-k materials. *Nat. Commun.* **2015**, *6*, 8700.

(13) Bauhofer, W.; Kovacs, J. Z. A review and analysis of electrical percolation in carbon nanotube polymer composites. *Compos. Sci. Technol.* **2009**, *69*, 1486−1498.

(14) Pei, S.; Cheng, H.-M. The reduction of graphene oxide. *Carbon* **2012**, *50*, 3210−3228.

(15) Chua, C. K.; Pumera, M. Reduction of graphene oxide with substituted borohydrides. *J. Mater. Chem. A* **2013**, *1*, 1892−1898.

(16) Shin, H.-J.; Kim, K. K.; Benayad, A.; Yoon, S.-M.; Park, H. K.; Jung, I.-S.; Jin, M. H.; Jeong, H.-K.; Kim, J. M.; Choi, J.-Y.; Lee, Y. H. Efficient Reduction of Graphite Oxide by Sodium Borohydride and Its Effect on Electrical Conductance. *Adv. Funct. Mater.* **2009**, *19*, 1987−1992.

(17) Banfi, L.; Narisano, E.; Riva, R.; Stiasni, N.; Hiersemann, M.; Yamada, T.; Tsubo, T. Sodium Borohydride. *Encyclopedia of Reagents for Organic Synthesis*; John Wiley & Sons, Ltd., 2001.

(18) Potts, J. R.; Shankar, O.; Du, L.; Ruoff, R. S. Processing−morphology−property relationships and composite theory analysis of reduced graphene oxide/natural rubber nanocomposites. *Macromolecules* **2012**, *45*, 6045−6055.

(19) Warner, J. H. Introduction. *Graphene*; Elsevier, 2013; Chapter 1, pp 1−4.

(20) Banfi, L.; Narisano, E.; Riva, R.; Stiasni, N.; Hiersemann, M. Sodium Borohydride. *Encyclopedia of Reagents for Organic Synthesis*; John Wiley & Sons, Ltd., 2001.

(21) Wu, Q.; Sundborg, H.; Andersson, R. L.; Peuvot, K.; Guex, L.; Nilsson, F.; Hedenqvist, M. S.; Olsson, R. T. Conductive biofoams of wheat gluten containing carbon nanotubes, carbon black or reduced graphene oxide. *RSC Adv.* **2017**, *7*, 18260−18269.

(22) Mott, P. H.; Roland, C. M. Limits to Poisson's ratio in isotropic materials. *Phys. Rev. B: Condens. Matter Mater. Phys.* **2009**, *80*, 132104.

(23) Guex, L. G.; Sacchi, B.; Peuvot, K. F.; Andersson, R. L.; Pourrahimi, A. M.; Ström, V.; Farris, S.; Olsson, R. T. Experimental review: chemical reduction of graphene oxide (GO) to reduced graphene oxide (rGO) by aqueous chemistry. *Nanoscale* **2017**, *9*, 9562−9571.

(24) Dave, K.; Park, K. H.; Dhayal, M. Two-step process for programmable removal of oxygen functionalities of graphene oxide: functional, structural and electrical characteristics. *RSC Adv.* **2015**, *5*, 95657−95665.

(25) Unalan, I. U.; Wan, C.; Figiel, Ł.; Olsson, R. T.; Trabattoni, S.; Farris, S. Exceptional oxygen barrier performance of pullulan nanocomposites with ultra-low loading of graphene oxide. *Nanotechnology* **2015**, *26*, 275703.

(26) Ganguly, A.; Sharma, S.; Papakonstantinou, P.; Hamilton, J. Probing the Thermal Deoxygenation of Graphene Oxide Using High-Resolution In Situ X-ray-Based Spectroscopies. *J. Phys. Chem. C* **2011**, *115*, 17009−17019.

(27) Yang, D.; Velamakanni, A.; Bozoklu, G.; Park, S.; Stoller, M.; Piner, R. D.; Stankovich, S.; Jung, I.; Field, D. A.; Ventrice, C. A.; Ruoff, R. S. Chemical analysis of graphene oxide films after heat and chemical treatments by X-ray photoelectron and Micro-Raman spectroscopy. *Carbon* **2009**, *47*, 145−152.

(28) Stankovich, S.; Dikin, D. A.; Piner, R. D.; Kohlhaas, K. A.; Kleinhammes, A.; Jia, Y.; Wu, Y.; Nguyen, S. T.; Ruoff, R. S. Synthesis of graphene-based nanosheets via chemical reduction of exfoliated graphite oxide. *Carbon* **2007**, *45*, 1558−1565.

(29) Mattevi, C.; Eda, G.; Agnoli, S.; Miller, S.; Andre Mkhoyan, K.; Celik, O.; Mastrogiovanni, D.; Granozzi, G.; Garfunkel, E.; Chhowalla, M. Evolution of Electrical, Chemical, and Structural

DOI: 10.1021/acsomega.8b03630
ACS Omega 2019, 4, 3458−3468

Properties of Transparent and Conducting Chemically Derived Graphene Thin Films. *Adv. Funct. Mater.* **2009**, *19*, 2577−2583.
(30) Bagri, A.; Mattevi, C.; Acik, M.; Chabal, Y. J.; Chhowalla, M.; Shenoy, V. B. Structural evolution during the reduction of chemically derived graphene oxide. *Nat. Chem.* **2010**, *2*, 581.
(31) Akhavan, O. The effect of heat treatment on formation of graphene thin films from graphene oxide nanosheets. *Carbon* **2010**, *48*, 509−519.
(32) Jeong, H.-K.; Lee, Y. P.; Lahaye, R. J. W. E.; Park, M.-H.; An, K. H.; Kim, I. J.; Yang, C.-W.; Park, C. Y.; Ruoff, R. S.; Lee, Y. H. Evidence of Graphitic AB Stacking Order of Graphite Oxides. *J. Am. Chem. Soc.* **2008**, *130*, 1362−1366.
(33) Barinov, A.; Gregoratti, L.; Dudin, P.; La Rosa, S.; Kiskinova, M., Imaging and Spectroscopy of Multiwalled Carbon Nanotubes during Oxidation: Defects and Oxygen Bonding (Adv. Mater. 19/2009). *Adv. Mater.* **2009**, *21* (), n/a-n/a. DOI DOI: 10.1002/adma.200990067.
(34) Gao, W.; Alemany, L. B.; Ci, L.; Ajayan, P. M. New insights into the structure and reduction of graphite oxide. *Nat. Chem.* **2009**, *1*, 403.
(35) Fakhru'l-Razi, A.; Atieh, M. A.; Girun, N.; Chuah, T. G.; El-Sadig, M.; Biak, D. R. A. Effect of multi-wall carbon nanotubes on the mechanical properties of natural rubber. *Compos. Struct.* **2006**, *75*, 496−500.
(36) Jacob, M.; Thomas, S.; Varughese, K. T. Mechanical properties of sisal/oil palm hybrid fiber reinforced natural rubber composites. *Compos. Sci. Technol.* **2004**, *64*, 955−965.
(37) Ren, Y.; Shui, H.; Peng, C.; Liu, H.; Hu, Y. Solubility of elemental sulfur in pure organic solvents and organic solvent−ionic liquid mixtures from 293.15 to 353.15K. *Fluid Phase Equilib.* **2011**, *312*, 31−36.
(38) Wang, S.; Zhang, X.; Wu, X.; Lu, C. Tailoring percolating conductive networks of natural rubber composites for flexible strain sensors via a cellulose nanocrystal templated assembly. *Soft Matter* **2016**, *12*, 845−852.
(39) Kuilla, T.; Bhadra, S.; Yao, D.; Kim, N. H.; Bose, S.; Lee, J. H. Recent advances in graphene based polymer composites. *Prog. Polym. Sci.* **2010**, *35*, 1350−1375.
(40) Potts, J. R.; Dreyer, D. R.; Bielawski, C. W.; Ruoff, R. S. Graphene-based polymer nanocomposites. *Polymer* **2011**, *52*, 5−25.
(41) Lin, Y.; Liu, S.; Chen, S.; Wei, Y.; Dong, X.; Liu, L. A highly stretchable and sensitive strain sensor based on graphene-elastomer composites with a novel double-interconnected network. *J. Mater. Chem. C* **2016**, *4*, 6345−6352.
(42) Nah, C.; Lim, J. Y.; Cho, B. H.; Hong, C. K.; Gent, A. N. Reinforcing rubber with carbon nanotubes. *J. Appl. Polym. Sci.* **2010**, *118*, 1574−1581.
(43) Ponnamma, D.; Sadasivuni, K. K.; Strankowski, M.; Guo, Q.; Thomas, S. Synergistic effect of multi walled carbon nanotubes and reduced graphene oxides in natural rubber for sensing application. *Soft Matter* **2013**, *9*, 10343−10353.

DOI: 10.1021/acsomega.8b03630
ACS Omega 2019, 4, 3458−3468